Plume-Induced Delamination Initiated at Rift Zones on Venus

Andrea C. Adams[1] , Dave R. Stegman[1], Hiva Mohammadzadeh[2], Suzanne E. Smrekar[3], and Paul J. Tackley[4]

[1]Institute of Geophysics and Planetary Physics, Scripps Institution of Oceanography, University of California San Diego, San Diego, CA, USA, [2]University of California, Berkeley, Berkeley, CA, USA, [3]Jet Propulsion Laboratory, California Institute of Technology, Pasadena, CA, USA, [4]Department of Earth Sciences, Institute of Geophysics, ETH Zürich, Zürich, Switzerland

Abstract Venus' tectonic evolution is not well understood. Thousands of kilometers of possible subduction sites on Venus have been identified along networks of rift zone trenches called chasmata. Rift zones are strong candidates for tectonic recycling due to pre-existing weaknesses in the lithosphere. Recently, peel-back delamination (PBD) was proposed as a mechanism of regional-scale lithospheric recycling initiated at Venusian rift zones (Adams et al., 2022, https://doi.org/10.1029/2022je007460). PBD occurs when the lithospheric mantle becomes sufficiently thick and negatively buoyant to decouple and peel away from the overlying crust remaining at the surface. Both positively and negatively buoyant lithosphere were shown to undergo buoyancy-driven PBD, though delamination is inhibited by increasing positive plate buoyancy. In this study, we use 2D numerical models to verify that delamination can be initiated in thinner, more positively buoyant lithosphere than in models with no plume-rift interactions. Our results show that plume-induced PBD in positively buoyant plates is facilitated by the excess negative buoyancy in the lithospheric mantle and increasing plume buoyancy force, and it is inhibited by increasing crustal buoyancy and decreasing rift width. We propose an age-progressive framework for delamination at rift zones, where young, thin plates require a larger plume buoyancy force to be destabilized than thicker, yet still positively buoyant plates. We use lithospheric thickness constraints to predict PBD may be most likely to initiate near the Dali-Diana Chasmata system.

Plain Language Summary Venus' tectonic evolution is not well understood. Long networks of rift zone trenches called chasmata have previously been identified as potential locations of tectonic recycling due to their pre-existing lithospheric weaknesses. Peel-back delamination (PBD) was recently proposed as a potential mechanism of regional-scale lithospheric recycling on Venus, in which dense, trench-adjacent lithospheric mantle detaches and "peels away" from the overlying layer of buoyant crust remaining at the surface. In this study, we use 2D numerical models to further investigate the conditions in which delamination may operate in chasma rift zone environments on Venus by considering complexities from plume-rift interactions. We find that increasing plume radius, and thereby buoyancy force, results in PBD events in increasingly positively buoyant lithosphere compared to non-plume models. Increasing rift width and decreasing crustal density also facilitate delamination. An age-progressive framework is proposed for delamination at rift zones, where young, thin plates require a larger plume buoyancy force to be destabilized than thicker, yet still positively buoyant plates. We use lithospheric thickness constraints to predict PBD may be most likely to initiate near the Dali-Diana Chasmata system.

1. Introduction

It is generally agreed that Venus does not have Earth-like plate tectonics. Unlike Earth, Venus lacks a global, continuous system of crust formation at mid-ocean ridges and lithospheric recycling at subduction zones (Solomon et al., 1992). Despite having a diverse surface of volcanic plains, highly deformed tesserae, highland regions, chasma rift zones, and quasi-circular structures called coronae, Venus is typically categorized as a stagnant-lid planet (Solomatov & Moresi, 1996), where the mantle is actively convecting beneath an effectively single-plate lithosphere with no clear system of plate boundaries. This raises the question of how Venus has evolved over time, given that the surface is estimated to be relatively young (240–800 Myr) on geologic timescales (Feuvre & Wieczorek, 2011; McKinnon et al., 1997; Phillips et al., 1991). Following NASA's Magellan mission, two competing theories emerged to describe the potential resurfacing styles of Venus: (a) the catastrophic resurfacing hypothesis predicts nearly all of the lithosphere was recycled into the mantle during one or more discrete tectonic events (Armann & Tackley, 2012; Bullock et al., 1993; Parmentier & Hess, 1992; Romeo & Turcotte, 2009;

Schaber et al., 1992; Strom et al., 1994; Turcotte, 1993), whereas (b) the regional equilibrium resurfacing (RER) hypothesis predicts resurfacing is a combination of regional-scale processes occurring throughout time that may result from a variety of tectonic and volcanic mechanisms (Bjonnes et al., 2012; O'Rourke et al., 2014; Phillips et al., 1991, 1992).

Across Venus, the tendency of the lithospheric mantle to sink is in constant competition with a layer of crust that is compositionally less dense than mantle and adds significant positive buoyancy to the plate. Admittance spectra calculated from gravity and topography data reveal regional variations in crust and lithosphere thickness, with lithosphere thickness estimates ranging from 7 to 284 km (Smrekar et al., 2022) and crustal thicknesses between 0 and 100 km (Anderson & Smrekar, 2006). Estimates of the global average crustal thickness on Venus fall between 20 and 30 km (James et al., 2013; Jiménez-Díaz et al., 2015; Simons et al., 1997), which adds substantially more positive buoyancy to the lithosphere than oceanic crust of subducting plates on Earth. Calculations of the density defect thickness (Oxburgh & Parmentier, 1977) versus cooling age indicate that lithosphere with 8 km of oceanic crust on Earth will become negatively buoyant after 40 Myr; yet lithosphere on Venus with 24 km of crust is predicted to remain gravitationally stable up to 550 Myr (Schubert & Sandwell, 1995) with other estimates as low as 300 Myr (Parmentier & Hess, 1992). While the potential agreement between this threshold age for gravitational instability and the estimated surface age of Venus may be used to argue in favor of a global overturn resurfacing event, evidence for strong lithospheric heterogeneity (Smrekar et al., 2022) and globally inconsistent net plate buoyancy on Venus may be indicative of a more complex resurfacing model. A major question in Venusian tectonics is whether, similar to subduction on Earth, negative plate buoyancy is a requirement for lithospheric recycling; if not, how can positively buoyant plates on Venus be recycled?

A popular conceptual model for coronae formation is plume-induced subduction, which is thought to occur when a rising mantle plume penetrates the lithosphere and pushes the plate edges downward into the mantle from above, creating an annular retreating trench (Sandwell & Schubert, 1992a, 1992b). In theory, subduction can occur despite the plate initially being positive buoyant because crustal density increases at the basalt-eclogite transition during the magma loading stage, and a higher-density eclogite layer may help sustain subduction (Gülcher et al., 2020; Sandwell & Schubert, 1992a). Plume-induced subduction via surface loading has been validated in laboratory tank experiments (Davaille et al., 2017), though the thickness and density of the crust were unable to be controlled independently. While lithosphere that is too thick may hinder plume penetration, lithosphere that is too thin may be unable to support viscous plate bending and subduction. Lithospheric flexure near coronae is generally associated with relatively small elastic thicknesses (<20 km) and high heat flow, indicating that most coronae may preferentially form on thin lithosphere (O'Rourke & Smrekar, 2018; Smrekar et al., 2022), yet the smaller subset of coronae showing evidence of plume-induced subduction typically occur in relatively older, thicker lithosphere aged between 25 and 140 Myr (Sandwell & Schubert, 1992a). The plume-induced subduction mechanism has only been modeled for a spherical plume embedded at shallow depths beneath a thin lithosphere (30 km crust + 15 km lithospheric mantle) (Gülcher et al., 2020), and it is unclear how a rising plume would interact with, and potentially recycle, older and thicker lithosphere.

Delamination may be an alternative mechanism of recycling thick, yet positively buoyant lithosphere on Venus, particularly near chasmata which have pre-existing lithospheric fractures and abundant coronae, many of which likely form above small-scale plumes. Subduction and delamination are sometimes used in the literature interchangeably, but here we differentiate between the two terms: subduction involves significant crustal recycling, whereas delamination refers to only partial lithospheric recycling, either by lithospheric dripping (Göğüş et al., 2017; Hoogenboom & Houseman, 2006; Houseman & Molnar, 1997) or by decoupling of the lithospheric mantle along the Moho (Bird, 1979; Chowdhury et al., 2020; Göğüş & Ueda, 2018; Krystopowicz & Currie, 2013; Magni et al., 2013; Meissner & Mooney, 1998). Delamination of the lower lithosphere has been suggested as a mechanism for heat loss resulting from plume-lithosphere interactions on Venus (Ashwal et al., 1988; Smrekar & Stofan, 1997). However, the idea of regional-scale delamination has mostly been applied to Earth, including in the northwest US (Darold & Humphreys, 2013) and the Rwenzori mountains in Africa (Wallner & Schmeling, 2010).

Adams et al. (2022) modeled a specific delamination mechanism called "peel-back delamination" (PBD) at a chasma-like rift margin on Venus which resulted in the full sub-crustal lithospheric mantle being recycled on a regional-scale. PBD occurs when the negatively buoyant lithospheric mantle decouples and peels away from the positively buoyant, overlying crust along the Moho. Following a PBD event, a hot, thinned layer of

deformed crust remains at the surface. Peel-back delamination driven solely by lateral density contrasts across a pre-existing lithospheric fracture, or buoyancy-driven PBD, was observed for both positively and negatively buoyant lithosphere (Adams et al., 2022). It is primarily dependent on the thickness of the lithospheric mantle, which defines the extent of its negative thermal buoyancy. Buoyancy-driven PBD consistently occurred in models with 300-km-thick lithosphere, despite having a net-positive buoyancy from 30 km of positively buoyant crust. Conversely, all cases with a positively buoyant 200-km-thick lithosphere resulted in a stagnant-lid due to having insufficient negative buoyancy in the lithosphere mantle; this was true even when crustal density was adjusted to yield the same net plate buoyancy as the 300 km lithosphere delamination models. Between these two endmember scenarios, delamination in 250-km-thick lithosphere was dependent on crustal density, with PBD requiring reduced crustal buoyancy to go unstable.

To isolate the effects of plate buoyancy on the PBD mechanism, Adams et al. (2022) did not consider the role of plume-rift interactions; however, rift zones on Venus may require this additional complexity. Small compensation depths (Smrekar et al., 2010) and a geoid gradient and stress field orientation consistent with a swell-push model (Sandwell et al., 1997) do not support the existence of a large broad-scale active upwelling below any of the large chasma; instead, chasmata may be strongly associated with localized plume activity, as evidenced by high heat flows (Smrekar et al., 2022) and a relatively high density of coronae at certain chasmata (Glaze et al., 2002; Smrekar et al., 2010). While the mechanisms for corona formation are not well understood and may include non-plume origins (Hoogenboom & Houseman, 2006; McGovern et al., 2013; Tackley & Stevenson, 1991), the majority of models attribute corona formation either directly or indirectly to interactions between the lithosphere and a mantle upwelling (Davaille et al., 2017; Dombard et al., 2007; Gerya, 2014; Gülcher et al., 2020; Janes, 1992; Koch & Manga, 1996; Piskorz et al., 2014; Smrekar & Stofan, 1997; Squyres et al., 1992; Stofan et al., 1991, 1992). The next step in understanding delamination initiated at rift zones on Venus is to consider whether adding a rising mantle plume could destabilize the lithospheric mantle and trigger PBD in even younger, more positively buoyant plates than was possible for purely buoyancy-driven subduction. It is unclear how a plume would affect the mechanism of delamination initiation, and whether the outcome would be some form of delamination, subduction, or obstruction of lithospheric recycling due to the uplifting force of a rising plume.

In this study, we use 2D numerical models to investigate the dynamics of plume-rift interactions and the consequences for delamination initiation. We systematically vary lithosphere thickness, crustal density, plume radius, and width of the rift zone to identify the conditions where PBD may be a viable mechanism for regional-scale lithospheric recycling within the context of the RER hypothesis. We propose a new framework for plume-assisted lithospheric recycling at rift zones on Venus which is primarily dependent on lithospheric thickness and plume radius. We then identify specific rift zones on Venus where our models indicate delamination may be most likely to occur.

2. Model Setup

We performed a series of 2D numerical simulations using StagYY, a finite volume code used to model planetary-scale convection problems (Crameri et al., 2017; Tackley, 2008). All post-processing and visualization was performed using StagLab 6.0 (Crameri, 2018, 2021). Additional details of the code and model setup are described in Adams et al. (2022). Like Adams et al. (2022), the initial condition is a 180° half-spherical annulus geometry with a simplified rift zone, which is modeled as a horizontal lithospheric gap separating two plate edges with a maximum viscosity of 10^{24} Pa*s (Figure 1). The lithospheric thickness to the left of the gap is varied between $h_L = [150, 200, 250]$ km. To the right of the gap, the lithosphere is 100 km thick and gradually thickens to a value of h_L at a distance of 2,100 km from the rift zone. We use a constant crust thickness ($h_c = 30$ km), but vary the compositional buoyancy of the crust with respect to the reference mantle density ($B_{crust} = \rho_{0,crust} - \rho_0 = [-265, -300, -350, -400]$ kg/m³) to control crustal buoyancy. For example, 30 km of crust with $B_{crust} = -265$ kg/m³ represents the same amount of crustal buoyancy as a 20 km crust with a density anomaly of $B_{crust} = -400$ kg/m³. Previously in Adams et al. (2022), the gap was kept a constant width of $L_{gap} = 250$ km in order to minimize the stabilizing effect a smaller gap size could have on spontaneous, buoyancy-driven lithospheric recycling events. To further investigate the role that rift zone geometry may play in delamination initiation, we now vary the width of the rift zone, L_{gap}, between 250, 125, and 60 km (Figure S1 in Supporting Information S1), which is compatible with observations of chasma trench width on Venus (Martin et al., 2007; Schubert & Sandwell, 1995). We ignore the effects of plume cooling as it rises through the warm mantle prior to reaching the surface, since the timescales of cooling are on the order of 100s of millions of years (Koch & Manga, 1996).
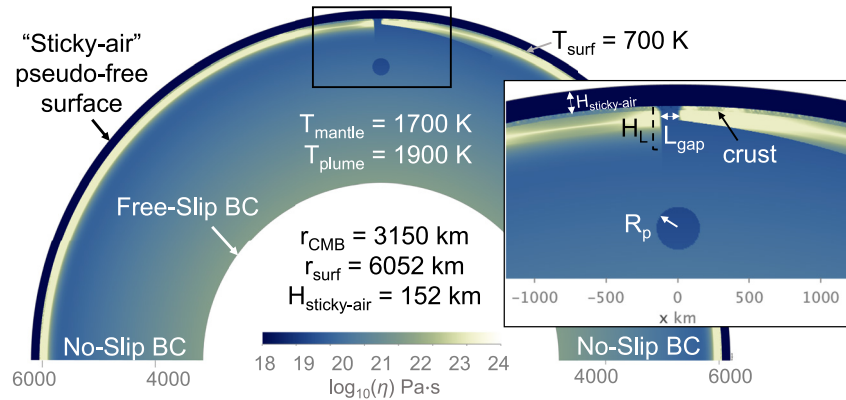
Figure 1. Initial model setup in the viscosity field. Rift width (L_{gap}) is varied between 60, 125, and 250 km, but shown here is a 125 km-wide rift gap (see Figure S1 in Supporting Information S1 for further details). Plume radius ($R_p = 150$ km shown here) and lithospheric thickness of the left plate edge ($H_L = 250$ km here, defined by 1600 K isotherm) are also varied between models. The thickness of the plate edge to the right of the rift gap is fixed at 100 km and gradually increases to H_L over a distance of 2,100 km from the rift. The distance from the surface to the top of the plume head is 700 km regardless of plume size. At the surface, a continuous layer of buoyant crust ($H_c = 30$ km) with variable density (B_{crust}) covers the lithosphere and the rift gap. Above the surface, 152 km of low-viscosity sticky-air is used as a pseudo-free surface boundary condition to allow the development of realistic topography.

In order to better understand rift zone destabilization, we incorporated a purely thermal mantle plume below the gap. The radius of the plume, R_p, was varied in order to investigate a range of plume buoyancy forces. The buoyancy force, F_B, of a circular plume is given as:

$$F_B = \pi R_p^2 \Delta\rho g \tag{1}$$

where g is gravitational acceleration and the density anomaly of a thermal plume, $\Delta\rho$, is defined by:

$$\Delta\rho = \rho_{p,0} \alpha \Delta T \tag{2}$$

where $\rho_{p,0}$ is the density of the plume at the ambient mantle temperature, T_m, α is the coefficient of thermal expansion, and ΔT is the temperature anomaly of the plume with respect to T_m. We hypothesize the buoyancy force of the plume will play an important role in destabilizing the lithosphere adjacent to the rift gap; however, it is important to keep in mind that a limitation of the 2D spherical annulus geometry (x, z) is that both the lithosphere and plume represent infinitely long features in the in the y-direction. As a result, our calculated plume buoyancy force is only an approximation. We adopt a modest temperature contrast of only 200 K, which may represent the small temperature drops that occur across the core-mantle boundary in stagnant-lid planets (Thiriet et al., 2019). Although plume temperature could also be used to vary the plume buoyancy force, we used a constant mantle and plume temperature in order to maintain a constant viscosity contrast ($T_m = 1700$ K, $\Delta T = 200$ K). The plume is always centered below the edge of the plate to the right of the gap, and the top of the plume head is initially positioned at a depth of 700 km to ensure a realistic plume shape and rise velocity as it encounters the lithosphere and rift zone.

3. Results

Of the 49 total models that were run, 32 models resulted in a plume-induced PBD event. These 32 delamination models described in the following sections are divided into three subgroups based on the ratio of plume radius to rift gap width, R_p/L_{gap}. The remaining 16 models were classified in the stagnant-lid tectonic regime, which is characterized by a lack of significant horizontal or vertical surface displacement of the lithosphere throughout the model evolution. No other model outcomes were observed. A summary of the parameter space and model outcomes is given in Tables S1 and S2 in Supporting Information S1.

3.1. Plume-Induced Peel-Back Delamination

3.1.1. Type I: Plume Radius ≈ Gap Width

A representative plume-induced PBD event is shown in Figure 2 for a reference model with a 250-km-radius plume rising into a 200-km-thick lithosphere with a 250-km-wide gap and a crustal density anomaly of
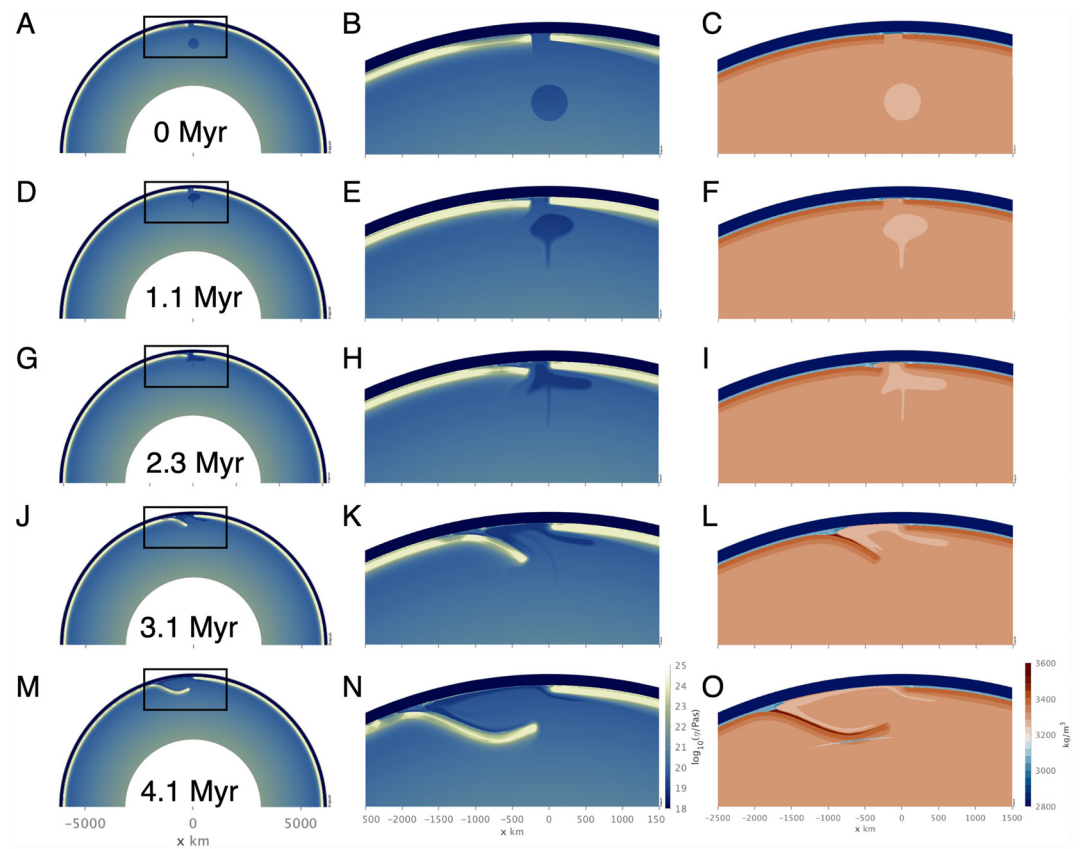
Figure 2. A typical plume-induced peel-back delamination event shown in the global viscosity field, local viscosity field, and local density field ($h_L = 200$ km, $L_{gap} = 250$ km, $R_p = 250$ km, and $B_{crust} = -300$ kg/m³). (a–c) The initial condition shows the location of plume and lithospheric gap. (d–f) The plume rises and flattens as it encounters the lithosphere. (g–i) The lithospheric mantle continues decoupling from the crust as the plume head rises into the gap and spreads beneath the right plate edge. (j–l) The lithospheric mantle peels away from the surface and (l) eclogite formation (dark red) in the base of the crustal root (light blue) helps sustain slab sinking. (m–o) The slab tip is deflected upward by regions of positive buoyancy in the slab due to Earth-like phase transitions beginning at 710 km depth.

$B_{crust} = -300$ kg/m³. The following description of the model evolution applies to all plume-induced PBD models where plume radius is similar in magnitude to the rift zone width. The top of the plume head is initially located 700 km below the surface and is centered directly beneath the edge of the right plate edge (Figures 2a–2c). As the plume rises, it develops a distinct plume head-tail structure, which flattens as it encounters higher viscosity mantle material at the base of the lithosphere. When the plume reaches the base of the gap, a small separation between crust and lithospheric mantle can be observed at the top edge of the left plate. The induced mantle flow from the rising plume pushes the gap material into the weak crustal layer, which initiates decoupling (Figures 2d–2f). Like in buoyancy-driven PBD, yielding in the crust forms a weak zone delamination surface allowing decoupling to propagate along the Moho (Figure 5). The plume head deforms as a portion of the plume rises directly into the gap, while part of the plume underplates the base of the right plate edge (Figures 2g–2i). The plume pushes into the left plate edge, but does not produce significant underplating of the lithospheric mantle as slab sinking progresses. Decoupling between the crust and lithospheric mantle continues, but it is still the ambient mantle from inside the gap rather than plume material that is wedged between them. The lithospheric mantle begins to peel away, and the plume head spreads into the space between the remaining layer of crust at the surface and the upper boundary of the delaminating slab (Figures 2j–2l). The slab tip is deflected upward by the sources of positive buoyancy from phase changes beginning at 710 km depth (Figures 2m–2o) (see Adams et al. (2022) for details). The plate edge to the right of the gap (100 km thick) remained stable throughout all model evolutions.

In the early stages of decoupling, only a thin layer of crust approximately 5 km thick is attached to the down-going slab, while the majority of crust remains at the surface (Figure 2i). As the edge of the plate bends downward
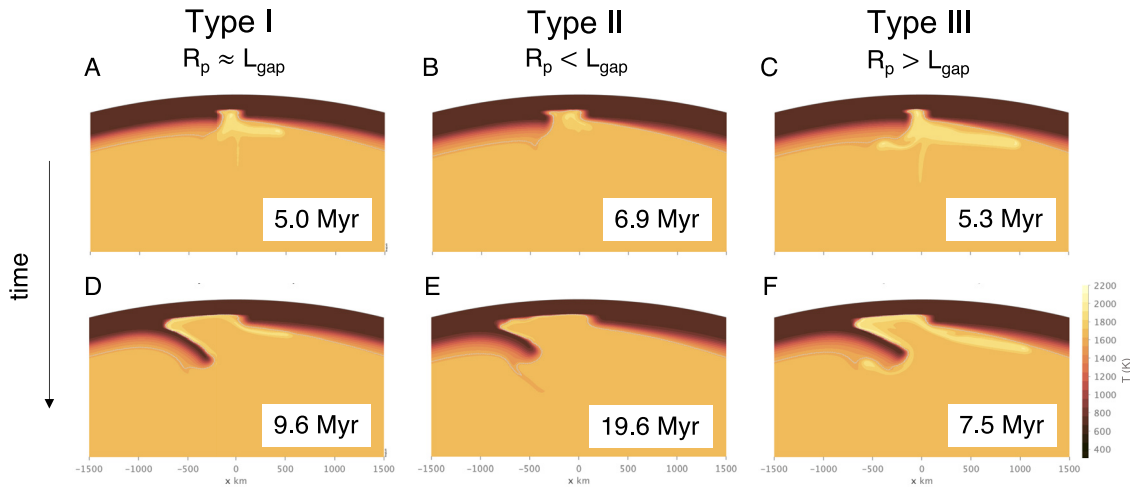
Figure 3. Temperature field progression of plume-induced peel-back delamination is given for the three types of plume-rift interactions. The 152 km-thick sticky-air layer covering the top of the lithosphere is the same temperature as the surface, and the top of the rift gap indicates the depth of the surface-air boundary. (a, d) Type I: plume radius is approximately equal to the gap width ($R_p = 150$ km, $L_{gap} = 125$ km) and there is only underplating of the right plate, (b, e) Type II: plume radius is much smaller than gap width ($R_p = 75$ km, $L_{gap} = 250$ km) and there is no underplating, and (c, f) Type III: plume radius is much larger than gap width ($R_p = 250$ km, $L_{gap} = 60$ km), and there is underplating of both plate edges. Note: Timing of delamination is also dependent on lithosphere thickness and crustal buoyancy, which is not constant between these three models.

into the mantle, a crustal root is formed at the slab hinge (Figure 2l). The base of the crustal root undergoes the basalt-eclogite phase transition at 70 km depth, resulting in higher density crustal material and an increase in crustal recycling. Nevertheless, the majority of crust remains at the surface and is deformed near the rift zone to accommodate the formation of the crustal root and the migration of the trench. There were no observed cases where eclogite formation occurred and PBD did not continue. Slab sinking is moderated by Earth-like phase transitions in the mid-mantle, which consistently results in stress focusing and break-off of a moderate-sized slab ($\approx 2,500$ km in length). Slab break-off is the final stage of a PBD event, and related details are discussed in Adams et al. (2022).

3.1.2. Type II: Plume Radius < Gap Width

When the ratio R_p/L_{gap} is approximately less than or equal to 0.5, the stages of plume-induced PBD progression are slightly different than described above. Smaller plumes take longer to reach the gap than larger plumes with a higher buoyancy force. Once the small plume encounters the edge of the right plate, it is deflected almost entirely into the gap, rather than underplating the right plate (Figure 3a). In some cases, the forces from the small plume entering the gap are able to induce crustal yielding and decoupling at the crust-mantle interface, which results in a similar evolution of PBD. The smaller plume diffuses into a very thin layer along the base of the crust, with the thickest layer of plume material being located above the plate hinge (Figure 3d). Although some cases of small plumes initiating delamination have been observed, many result in a stagnant-lid.

3.1.3. Type III: Plume Radius > Gap Width

When the ratio R_p/L_{gap} is greater than or equal to 2, only a small portion of the plume can rise into the empty gap space (Figure 3c). Whereas a small plume/large rift-gap combination only results in uplift of the right plate edge, a large plume also exerts an upward force beneath the delaminating plate edge when the gap is small. The positively buoyant excess plume material is spread beneath the lithosphere on both sides of the rift zone, further inhibiting plate bending and crustal yielding which is necessary for plate decoupling to occur; however, increasing plume size results in higher pressures in the gap which can facilitate decoupling at the base of the crust. Once decoupling begins, the excess negative buoyancy of the lithospheric mantle and eclogitized crust can drive the slab to sink despite the upward force on the plate edge from the plume. As the lithospheric mantle peels away, the large plume is spread into a relatively thick layer along the base of the right plate, the base of the crust in the gap, along the top of the delaminating slab, and around the slab tip.
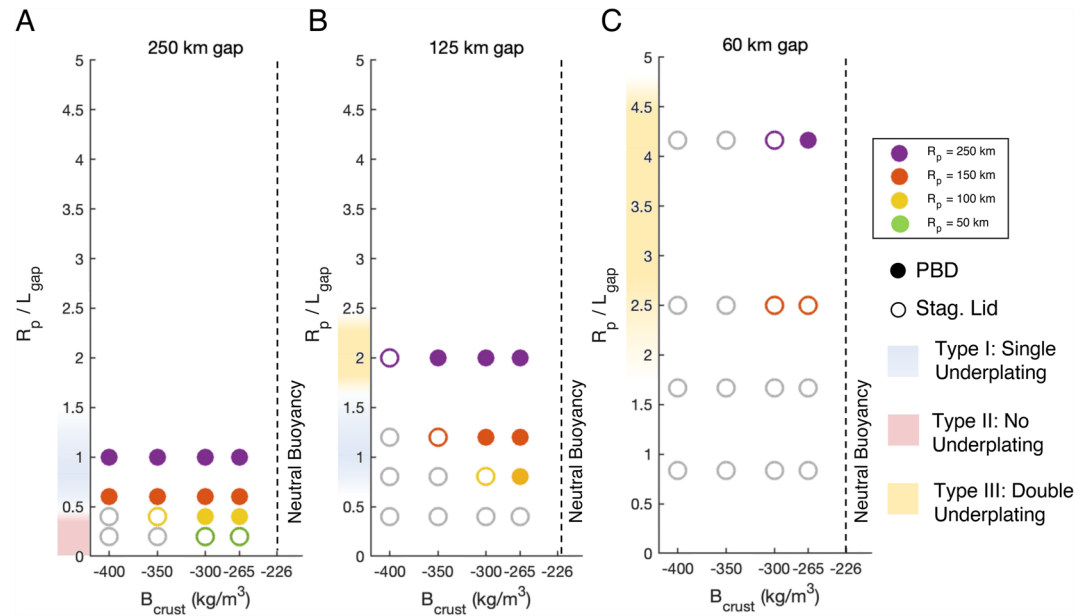
Figure 4. Model outcomes for 200-km-thick lithosphere with a (a) 250 km gap, (b) 125 km gap, and (c) 60 km gap plotted for the ratio of plume radius to gap width (R_p/L_{gap}) versus crustal density anomaly (B_{crust}). Unfilled gray circles are models inferred to be stagnant-lid based on the stabilizing effect of decreasing gap size and increasing positive crustal buoyancy (i.e., if a model is stagnant-lid, increasing positive crustal buoyancy and/or decreasing plume size can also be expected to remain stagnant-lid. We can also assume that if a model did not delaminate with a 50 km-radius plume with a 250 km-wide gap, it will also not delaminate with a 125 or 60 km-wide gap.). Colors on the *y*-axis indicate the style of plume-lithosphere interaction; (blue) Type I: the plume and gap are similar in size and underplating occurs below the right plate edge only, (red) Type II: The plume is small and enters gap without underplating, and (yellow) Type III: the plume is larger than gap and underplates both plate edges. All plates are positively buoyant, and increasing distance from the line of neutral buoyancy represents increasingly positive net plate buoyancy.

3.2. Effects of Plume Radius, Gap Width, and Crustal Buoyancy on Delamination Initiation

In Adams et al. (2022), all positively buoyant plates with 200-km-thick lithosphere were stagnant-lid, unable to undergo buoyancy-driven PBD. In Figure 4, we present the tectonic regime outcomes of either plume-induced
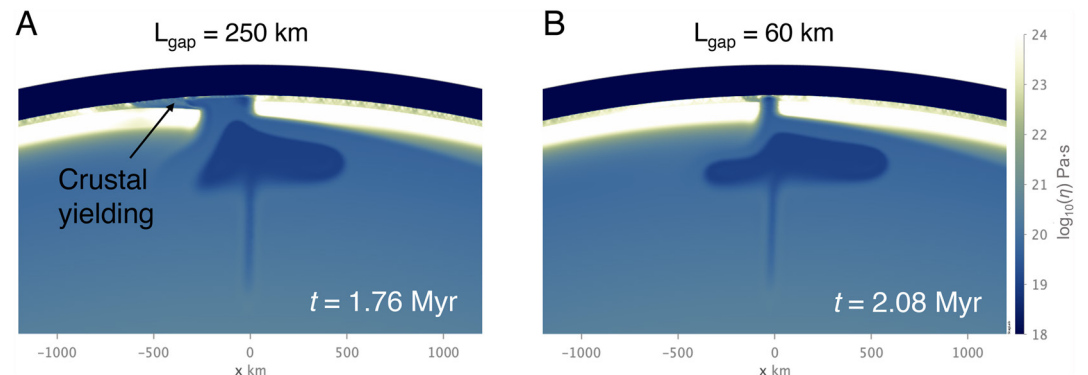

Figure 5. Delamination initiation requires crustal yielding and weakening above the delaminating plate edge to allow decoupling to propagate along the Moho (see Adams et al. (2022) for details). (a) For a 250 km-wide rift gap, there is minimal spreading of the plume beneath the delaminating plate. The plate edge is able to bend and induce stresses in the overlying crust which exceed the yield stress, and this allows delamination to progress, despite being stagnant-lid in the absence of plume interactions (Adams et al., 2022). (b) For a smaller gap width (60 km) and an increasing R_p/L_{gap} ratio, enhanced underplating of the buoyant plume exerts an upward force on the plate edge from below. This inhibits plate bending and crustal yielding, which ultimately results in a stagnant lid. The two models are identical ($R_{plume} = 250$ km, $h_L = 200$ km, $B_{crust} = -265$ kg/m^3) with the exception of gap width.

PBD (closed circles) or stagnant-lid (open circles) for various 200 km lithosphere models following interactions with a rising mantle plume. Using the same gap width as in Adams et al. (2022), L_{gap} = 250 km, relatively small plumes (R_p = 50 km) are unable to destabilize the rift zone, regardless of the crustal buoyancy of the plate (Figure 4a). Plume-induced PBD is observed after increasing plume radius to 100 km, but only in plates with the least positively buoyant crust (B_{crust} = [−265, −300] kg/m³). A stagnant-lid persists in models with lower density crust (B_{crust} = [−350, −400] kg/m³), indicating positive crustal buoyancy has a stabilizing effect on the rift zone. When the gap was large (L_{gap} = 250 km), plume-induced PBD was initiated for all plume radii greater than or equal to 150 km regardless of crustal buoyancy.

Gap width was held constant in previous models of buoyancy-driven delamination, but here we tested smaller gap sizes to determine its effect on rift zone stabilization. When gap width is decreased from 250 to 125 km, a 150-km-radius plume which previously always initiated delamination now results in a stagnant-lid at the highest crustal buoyancies (B_{crust} = [−350, −400] kg/m³) (Figure 4b). Increasing the plume radius to 250 km can destabilize more positively buoyant plates than the 150 km plume (B_{crust} = −350 kg/m³), but a stagnant-lid persists for the most positively buoyant crust (B_{crust} = −400 kg/m³). For an even smaller gap width of 60 km, all plumes smaller than 250 km resulted in a stagnant-lid outcome; only one model underwent plume-induced PBD, and it only occurred for a combination of the largest plume size (R_p = 250 km) and the least buoyant crust (B_{crust} = −265 kg/m³). Collectively, these data show a trend between decreasing gap width and increasing rift zone stability, particularly in cases with more positive crustal buoyancy.

Notably, both stagnant-lid and plume-induced PBD outcomes were observed for all three types of plume-rift interactions (see Sections 3.1.1–3.1.3). For an on-rift-axis plume, the style of plume-lithosphere interaction depends on the ratio of plume radius to gap width. A small plume rising directly into the gap (Type II) occurs when the R_p/L_{gap} ratio is small (<0.5) (Figure 4a). A plume that underplates the right plate edge and only slightly encounters the left plate edge (Type I) occurs when the R_p/L_{gap} ratio is approximately 0.5–1.5 (Figures 4a and 4b). When the R_p/L_{gap} ratio is greater than 1.5, the plume is large enough to underplate both sides of the rift while the upper part of the plume enters the gap (Figures 4b and 4c). Although the R_p/L_{gap} ratio may characterize the style of plume-rift interaction, the actual tectonic outcome is depending on plume radius, gap size, and crustal buoyancy. For each of the three types of plume-rift interactions, increasing plume size, increasing gap width, and decreasing crustal buoyancy all facilitate plume-induced PBD. Although the relationship between R_p/L_{gap} and the different types of plume-rift interactions applies to a plume centered below the right plate edge, these results provide a general idea of how plume-rift dynamics depend on plume size and subsurface lithospheric structure (see also Figure S2 in Supporting Information S1).

4. Discussion

4.1. Stagnant-Lid Scenarios

There are three scenarios that can result in a stagnant-lid outcome. The first is when the lithosphere is thin and lacks sufficient negative buoyancy in the sub-crustal lithospheric mantle to induce delamination, regardless of any added plume buoyancy forces. The majority of 150 km lithosphere models were stagnant-lid, with the exception of one model with an anomalously large plume (R_{plume} = 500 km) (see Figure S3 in Supporting Information S1). This is also why the 100 km-thick lithospheric mantle to the right of the rift gap remains stable in all models. The second is a type II plume-rift scenario when the plume is small ($R_p \approx$ < 100 km) and has an insufficient buoyancy force which is unable to drive decoupling between the crust and mantle lithosphere. These models were typically run for several millions of years after the plume reached the surface and had been weakened by additional thermal diffusion. The third stagnant-lid scenario occurred in cases with type III plume-rift scenario, where PBD was inhibited by a combination of high positive plate buoyancy (thinner lithosphere and/or more positively buoyant crust) and extensive plume underplating. The plumes remained in the gap and beneath the plate edges for millions of years after reaching the surface while continuously eroding the base of the lithosphere. These models were run until it was clear that thermal erosion had removed substantial negative buoyancy from the mantle lithosphere, which is a requirement for delamination to occur.

4.2. Viability of Plume-Induced Delamination on Venus

The thickness of the lithosphere is arguably the most important factor in determining whether PBD can occur or if the rift will remain in a stagnant-lid regime. Both buoyancy-driven and plume-induced PBD are primarily
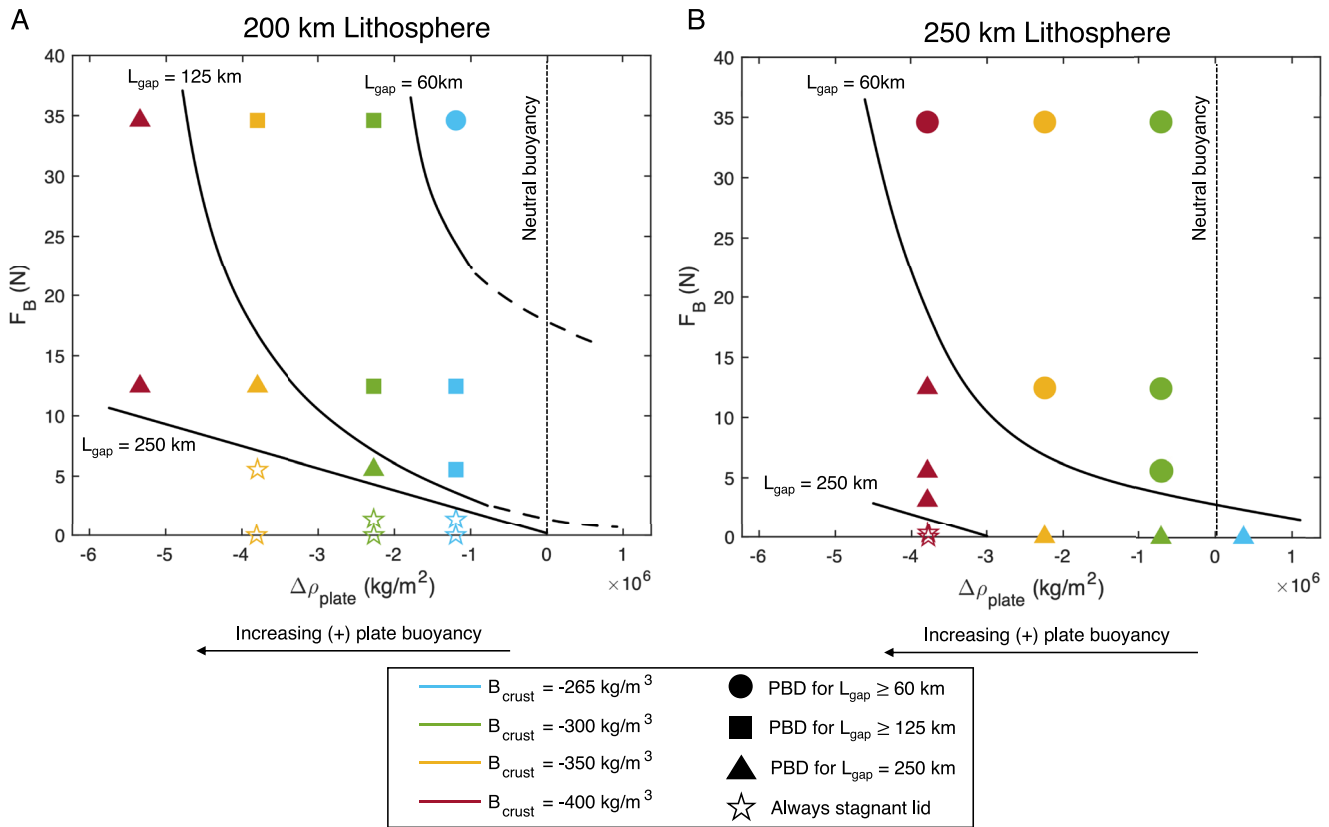
Figure 6. Tectonic regime diagrams for (a) 200-km-thick lithosphere and (b) 250-km-thick lithosphere. Solid lines indicate estimated location of regime boundaries. Dotted lines indicate extrapolated estimation of regime boundary behavior, based on evidence that negatively buoyant plates can also remain stagnant-lid when gap width is small and crustal buoyancy is weak. For reference, the outcomes of the non-plume models from Adams et al. (2022) are plotted along $F_B = 0$. The vertical dotted line at $\Delta\rho_{plate}$ is the line of neutral plate buoyancy—a negative $\Delta\rho_{plate}$ corresponds to a plate with a net positive integrated buoyancy. Without a plume, the most positively buoyant plate to undergo buoyancy-driven peel-back delamination (PBD) had a $\Delta\rho_{plate}$ of -2.24 kg/m² (Adams et al., 2022), but plume-induced PBD was observed for significantly more buoyant plates up to $\Delta\rho_{plate} = -5.34$ kg/m².

driven by the excess negative buoyancy of the lithospheric mantle, which becomes more negatively buoyant with increasing plate thickness and age. Adams et al. (2022) found that in buoyancy-driven PBD, bending of the dense lithospheric mantle induces extensional stresses in the overlying crust near the plate edge. When the stresses exceed the yield strength of the crust, the viscosity of the crust is reduced to an effective viscosity, forming a weak delamination surface which allows decoupling to propagate. Due to enhanced bending stresses, the thickest plates (300 km) were always able to undergo buoyancy-driven PBD without plume-assisted destabilization despite having a net positive plate buoyancy (Adams et al., 2022). Plume-induced PBD is initiated via the same mechanism of crustal yielding as buoyancy-driven PBD, and plume-rift interactions can increase crustal stresses and facilitate decoupling compared to models without a plume (Figure 5). Here, we found that 150-km-thick lithosphere did not delaminate for plumes (+200 K) up to 400 km in radius. The 150- and 300-km-thick lithosphere may represent minimum and maximum threshold values, respectively, which constrain the conditions where plume-induced PBD may operate for these rift geometries. The threshold thicknesses may shift to higher values depending on the structure of the rift zone, since narrowing gap widths has a stabilizing effect on the rift margin.

In this study, we focused on the range of lithosphere thicknesses where plume-induced PBD is most likely to operate. The model outcomes for 200- and 250-km-thick plates are shown in the parameter space of plume buoyancy force (F_B), a destabilizing force, versus the integrated density contrast between the plate and underlying mantle ($\Delta\rho_{plate} = \int_0^{h_L}(\rho(z) - \rho_0)\,dz$), which represents net plate buoyancy (Figure 6). Multiple regime boundaries are plotted as solid black lines based on gap width, where models above and to the right of the regime boundary are PBD. The dotted lines in Figure 6a are representative of an extrapolated regime boundary, based on evidence that positively buoyant plates can remain stagnant-lid for gap widths less than 250 km (Figure 6b), although the exact

shape of the regime boundary there is still unknown. Figure 6a shows that for the same gap width and crustal buoyancy, 200-km-thick plates require higher plume buoyancy forces for destabilization than the 250-km-thick plates in Figure 6b. Decreasing the gap width to 60 km has a stabilizing effect, particularly when combined with smaller plumes and more positively buoyant crust. Plume-induced PBD becomes less likely to occur with decreasing gap size, both due to the stabilizing nature of a more narrow weak zone and the increased probability that plume-rift interactions will result in underplating and uplift. As predicted, the 250 km lithosphere models undergo delamination more readily due to having a more negatively buoyant lithospheric mantle. The majority of 250 km lithosphere models (B_{crust} = [-265, -300, -350] kg/m^3) with a 250 km-wide gap did not require a plume for delamination to occur. Only a relatively small plume (R_p = 75 km) was necessary to destabilize the remaining stagnant-lid model (B_{crust} = -400 kg/m^3).

The relationship between positive plate buoyancy and the required plume buoyancy force to destabilize the rift is quasi-linear, indicating a force balance when the gap is large (L_{gap} = 250 km, Figure 6a) and there are minimal direct interactions between the plume and the left plate edge (Figure 4a). However as the gap width is decreased to 125 km, the required plume buoyancy force for delamination increases exponentially with increasing positive crustal buoyancy (decreasing $\Delta\rho_{plate}$). The change in the slope of the required buoyancy force may be a reflection of the shift from Type II to Type I and Type III plume-lithosphere interaction scenarios. When the plumes are relatively small ($F_B < 10$), there is no underplating or uplift below the delaminating plate edge (Type II). As the radius of the plume increases (F_B = 12.5, R_p = 150 km), the plume exerts a small upward force on the delaminating plate edge (Type I, Figure 3b). Although underplating alone is not sufficient to prevent delamination initiation, the combination of positive crustal buoyancy and plume uplift effectively work together to inhibit plate bending. When the plume is even larger (F_B = 34.6, R_p = 250 km), there is extensive uplift beneath the delaminating plate edge (Type III, Figure 3c). At this point, the slope of the regime boundary is much steeper, showing that positive crustal buoyancy has a more significant stabilizing effect when there is more underplating.

4.3. The Progression of PBD Mechanisms With Plate Age

In the absence of significant lithospheric extension or compression, the thickness of the lithospheric thermal boundary layer is primarily dependent on the age of the plate. We find that plume-induced PBD is less likely to occur when the lithosphere is less than 150 km thick, which corresponds to a plate age of 130 Myr. Buoyancy-driven PBD may be the dominant lithospheric recycling mechanism when the lithosphere is 300 km thick, or 625 Myr old, due to the significant negative buoyancy in the lithospheric mantle. Plume-induced PBD may be most applicable to zones of lithosphere on Venus that are between 130 and 625 Myr old and near a pre-existing weak zone, though plume destabilization may also be relevant for older lithosphere with more narrow, stable rift structures. Here, we modeled plume-induced PBD in lithospheres that were 300 and 450 Myr old (200 and 250 km thick, respectively). We observed that a larger plume was required to initiate PBD in younger, thinner lithosphere than in thicker lithosphere with more negative thermal buoyancy (Figure 6).

A large fraction of coronae on Venus may be preferentially associated with thin, rifted lithosphere (O'Rourke & Smrekar, 2018; Russell & Johnson, 2021; Smrekar et al., 2022). However, our results suggest that the PBD mechanism may not operate on Venus until the plate is moderately thick, corresponding to a minimum age between 130 and 300 Myr old depending on the radius of the plume. In Figure 7, we provide an interpretive summary of our results. If the lithosphere is younger than the minimum age and/or thinned via rifting, we expect no or minimal lithospheric recycling. As the lithosphere ages and thickens, or if a thick plate is weakened due to uplift-related lateral fracture propagation (Schubert & Sandwell, 1995), we expect plume-lithosphere interactions to preferentially result in PBD. However, if the plate is near the minimum threshold age for PBD, a larger plume buoyancy force (i.e., larger plume radius) is required to initiate delamination (Figures 7a–7c). As the lithosphere continues to age and thicken, smaller plumes with less buoyancy force can destabilize the lithosphere and initiate PBD because the driving force of PBD is greatly enhanced by increasing lithosphere thickness (Figures 7d–7i). Eventually when the lithosphere reaches the maximum threshold age between 450 and 625 Myr old, a plume will no longer be required, and buoyancy-driven PBD will be the dominate recycling mechanism provided the weak zone in the lithosphere persists (Figures 7j–7l).

4.4. Potential Delamination Sites on Venus

A global map of coronae locations show a relatively high concentration near the Beta-Atla-Themis (BAT) region where these three large volcanic rises are connected by three major rift zones: Parga, Hecate, and Devana
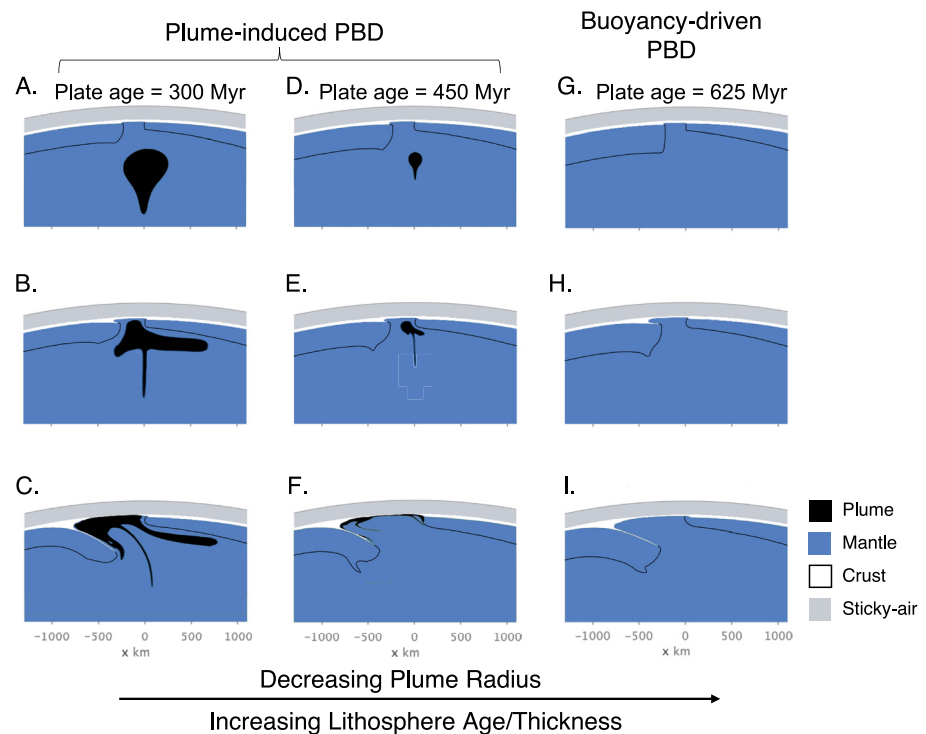
Figure 7. The dominant peel-back delamination (PBD) mechanism on Venus progresses from plume-induced to buoyancy-driven with increasing plate age. (a–c) Plume-induced delamination may occur once the minimum plate thickness has been reached (between 150 and 200 km thick, 130–300 Myr old) so that there is sufficient negative buoyancy in the lithospheric mantle. A larger plume buoyancy force is required to destabilize younger, less negatively buoyant plates (Figure 6). (d–f) As the plate ages and the lithospheric mantle becomes more negatively buoyant, comparatively smaller plumes can initiate PBD. (g–i) As the plate reaches 300 km thick (approximately 625 Myr old) a plume is no longer necessary to initiate delamination, since the lithospheric mantle is sufficiently dense to be gravitationally unstable in the absence of a plume perturbation. Plates thicker than 300 km can be expected to undergo buoyancy-driven delamination in the presence of a lithospheric weak zone.

Chasma (Figure 8a). Of the >500 coronae on Venus' surface, 131 are found in the Parga Chasma region (Martin et al., 2007). In theory, a high density of coronae may facilitate PBD initiation due to enhanced lithospheric perturbation; however the results of this study and Adams et al. (2022) demonstrate that sufficient negative buoyancy from a thick lithospheric mantle is the primary requirement for PBD. Low elastic thicknesses and higher than average heat flow estimates in the Parga rift zone and nearby coronae indicate that the lithosphere is thin with respect to a global average thickness of 70 ± 47.3 km (Smrekar et al., 2022). The trench geometry in the Parga Chasma system is highly variable, with trough widths measured between 80 and 200 km in the easternmost main branch and 50–250 km in the overlapping branches in its western end (Martin et al., 2007). Given that the minimum threshold lithosphere thickness to undergo PBD in our models is approximately 150–200 km (for $R_{plume} <= 250$–500 km, $L_{gap} <= 250$ km), Parga Chasma is unlikely to undergo regional-scale PBD in the near future despite its high density of coronae.

Of the possible subduction sites proposed by Schubert and Sandwell (1995), the Dali-Diana Chasmata system has the highest estimated plate bending moments (12.9e16 N, 12.4e16 N) and relatively high elastic thicknesses (34.3 km, 22.5 km) (Schubert & Sandwell, 1995). Within the Dali-Diana system, Artemis Corona and Atahensik (Latona) Corona also have relatively high plate bending moments (4.7e16 N, 6.4e16 N) and elastic thicknesses (34.6 km, 34.3 km) indicative of thicker lithosphere, thus making Dali and Diana Chasmata good candidates for PBD. Although there are fewer coronae in this region overall when compared to Parga Chasma (Figure 8a), this may be due to a filtering effect of the thicker lithosphere rather than an absence of mantle upwellings. Topography and lithospheric flexure surrounding Artemis Corona, the largest corona on Venus, indicates that it is a site of rollback lithospheric recycling where the trench is migrating radially outward to the south of Diana Chasma (Figure 8b) (Sandwell & Schubert, 1992a, 1992b), similar to the rollback delamination
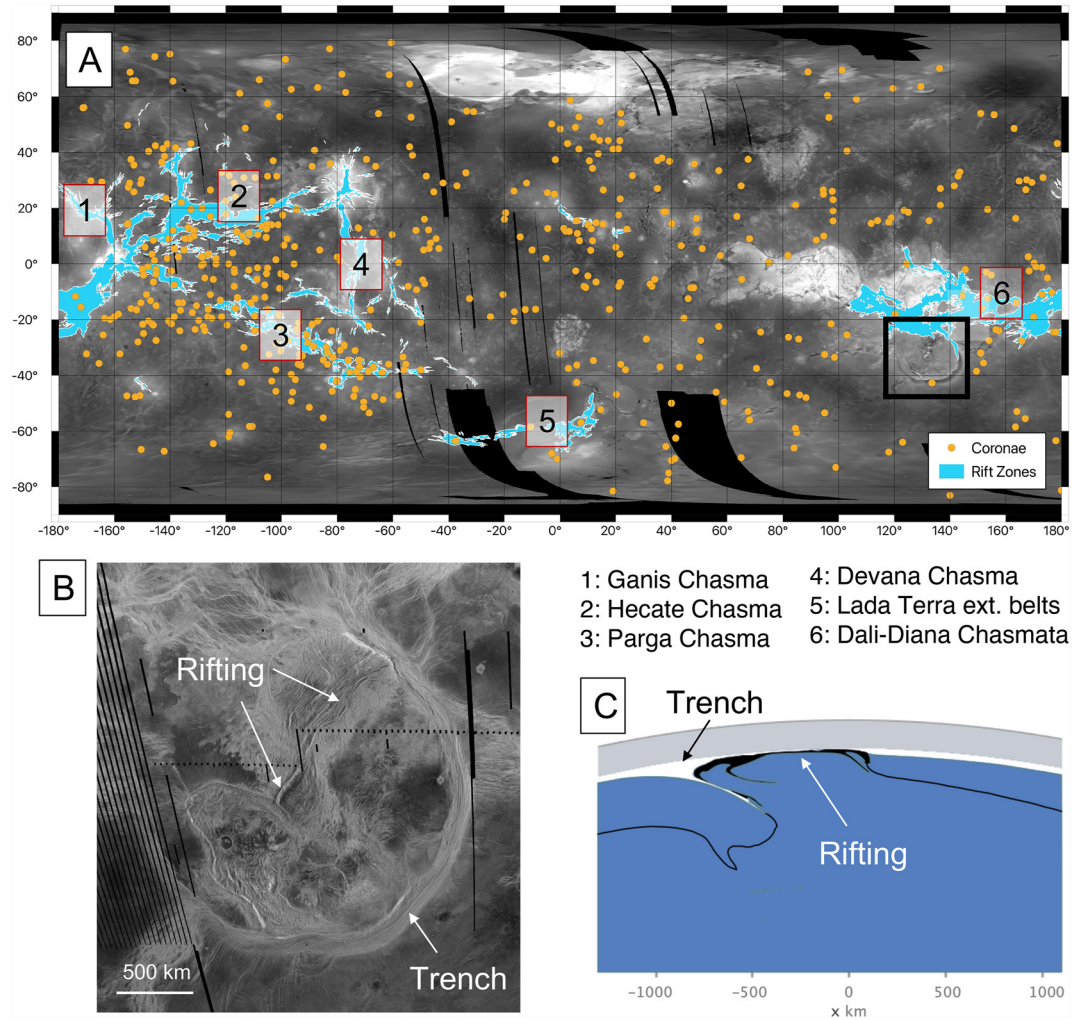
Figure 8. (a) Magellan global topography showing rift zones (Ivanov & Head, 2011) and approximately 500 coronae locations (Stofan et al., 1991). Six of the largest rift zones are labeled, five of which contain chasma trenches. The black box denotes Artemis Corona shown in panel (b). Artemis is characterized by a large arcuate trench thought to have migrated radially outward; it surrounds a highly deformed interior divided by linear bands of rifting. (c) In comparison, modeled plume-induced peel-back delamination events also display trench retreat causing rifting of thinned lithosphere in the center of the newly delaminated area (Figure 7f).

process shown by our models of PBD. A major feature of the highly deformed interior of Artemis is a band of lineated fractures inferred to be extensional rifting (Hansen, 2002; Spencer, 2001), and similar features have been generated in analog experiments of plume-induced subduction via magmatic loading (Davaille et al., 2017). Interestingly, we also observe crustal thinning and extensional rifting in the interior of the delaminated zone due to slab rollback and trench migration (Figure 8c). More work will be needed to model PBD in three dimensions to fully analyze surface topography and compare to Artemis Corona.

In our models, we implemented an asymmetrical lithospheric thickness across the rift zone so that the positive buoyancy of the thinner lithosphere would prevent a second concurrent delamination event from complicating our understanding of the delamination process. The results of this study and Adams et al. (2022) show that increasing the net positive buoyancy of the lithosphere inhibits delamination initiation, so by thinning the lithospheric mantle across the rift zone, we effectively removed negative buoyancy from the system. Opposite the rift zone from Artemis Corona, a large crustal plateau called Thetis Regio likely has a similar effect. Thetis Regio comprises a large portion of Aphrodite Terra, which is the largest highland terrain on Venus and is inferred to pre-date the formation of the Dali-Diana rift system (Basilevsky & Head, 1998; R. C. Ghail, 2002). The thickened crust on this side of the rift contributes significant positive buoyancy to the lithosphere which would likely

inhibit delamination initiation—similar to the effect of thinning the lithospheric mantle. As a result, delamination initiated at this section of Diana Chasma would likely only progress into its southern adjacent lithosphere rather than north into Aphrodite Terra.

4.5. Significance of Crustal Assumptions and Uncertainties

Constraining the thickness, density, and composition of Venus' crust is crucial to determining the viability of potential mechanisms of lithospheric recycling. Negative buoyancy in the lithospheric mantle is a driving force for all proposed forms of lithospheric overturn, whether it occurs regionally (buoyancy-driven PBD, plume-induced PBD, plume-induced subduction) or globally (catastrophic overturn). Similarly, a relatively thick layer of low-density crust on Venus may inhibit all proposed mechanisms of lithospheric recycling by increasing the positive buoyancy of the plate. To account for heterogeneity in crustal thickness (Anderson & Smrekar, 2006; James et al., 2013; Jiménez-Díaz et al., 2015), we varied crustal density over a range, B_{crust}, which gives a net positive buoyancy representative of various combinations of compositional density and crustal thickness.

Still, an incomplete understanding of Venus' crustal composition may lead to further uncertainties - in particular the depth of the basalt-eclogite transition. The formation of eclogite not only adds negative chemical buoyancy to the already negatively buoyant lithospheric mantle, but also removes positive buoyancy from the remaining layer of basaltic crust, thereby making it an important feature of lithospheric recycling on a potentially thick-crust planet such as Venus (Dupeyrat & Sotin, 1995). The few measurements of Venusian crust taken from the Venera 13, Venera 14, and Vega 2 missions indicate that the bulk composition of the crust at the landing sites resembles terrestrial basalt (Kargel et al., 1993; Surkov et al., 1984, 1986). However, uncertainties in both the composition as well as unknown parameters such as water content and oxygen fugacity can produce large variations in calculations of the Venusian basalt stability field, and subsequently, the depth of the basalt-eclogite transition. Variations in thermal gradient near rift zones (Smrekar et al., 2022) may also support a complex basalt-eclogite transition. Several recent studies of resurfacing on Venus have approximated the eclogite transition using experimental data of a tholeiitic Earth basalt stability field with a positive Clapeyron slope of $\approx$1.76 MPa/K (Ito & Kennedy, 1971), which yields a gradual eclogite transition depth beginning as shallow as 20–40 km (Gülcher et al., 2020; Tian et al., 2023). Conversely, Venus' high surface temperature combined with a shallow thermal gradient may cause eclogite formation to occur deeper in Venus' mantle than within Earth (James et al., 2013); it has been estimated to occur between 50 and 70 km depth and is often approximated an instantaneous density jump ($\gamma = 0$ MPa/K) near these depths (Armann & Tackley, 2012; Ogawa & Yanagisawa, 2014; Rolf et al., 2018; Uppalapati et al., 2020). More recently, P-T density maps calculated from the Vega 2 composition which assume full water saturation show a gradual transition to eclogite beginning at approximately 70 km depth and continuing at deeper depths (Chen et al., 2022). Here, we chose to model the eclogite transition as an instantaneous density jump ($\Delta\rho = 420$ kg/m^3, $\gamma = 0$ MPa/K) at 70 km depth, which helps sustain delamination but does not play a role in the early stages of its initiation. Going forward, it will be important to consider variations in the depth of the basalt-eclogite transition in order to understand the style and scale of lithospheric recycling possible for Venus. Depending on the local thermal gradient, the depth of the crust may overlap with the eclogite transition depth and result in shallower eclogite than previously expected. This would strongly affect the net lithospheric buoyancy which would have significant implications for the proposed modes of lithospheric recycling.

Finally, the yield strength of the crust is another parameter which is heavily debated, though not well constrained. We assume a weak crustal rheology (Arkani-Hamed, 1993; Buck, 1992; R. Ghail, 2015; Tian et al., 2023; Zuber, 1987) consistent with the effects of Peierls creep of a plagioclase rheology at the brittle-ductile transition (Azuma et al., 2014; Katayama, 2021). Yet in addition to experimental data supporting a relatively strong (yet weak compared to olivine) crustal rheology (Mackwell et al., 1998), numerical models of rift formation on Venus may also require a strong crust (Regorda et al., 2023). Though the PBD mechanism as we have modeled is reliant on the existence of a weak crustal layer ($C_0 = 10$ MPa), delamination events on Earth are thought to result from a variety of mechanisms other than crustal yielding, including melting and thermal weakening near the crust-mantle boundary (Faccenda et al., 2009; Ueda et al., 2012). Intrusive magmatism in Venus' lithosphere (Lourenço et al., 2020) may also facilitate full or partial lithospheric decoupling. The magmatic effects of plume-lithosphere interactions on Venus will also play a role (Schools & Smrekar, 2023), however this is not within the scope of this study.

5. Conclusions

Compared to buoyancy-driven PBD (Adams et al., 2022), delamination initiated by plume-rift interactions was found to be viable for thinner, more positively buoyant lithosphere on Venus. Though both mechanisms can result

in recycling of positively buoyant lithosphere, the upward force from a rising plume increases stresses in the crust adjacent to the rift gap, which facilitates decoupling of the lithospheric mantle from the overlying crust. Like buoyancy-driven PBD, plume-induced PBD is driven by the negative buoyancy of the lithospheric mantle and inhibited by positive crustal buoyancy. Increasing the plume buoyancy force by increasing plume radius is shown to have a destabilizing effect on the rift margin, particularly when the width of the rift is large. However, increasing plume size with a smaller rift width can cause a range of underplating scenarios which can hinder delamination initiation. Though the positive buoyancy of the crust alone may not be sufficient to prevent destabilization of the lithospheric mantle, an underplating plume may contribute to stabilization by uplifting the plate edge from below. The combination of underplating and high positive crustal buoyancy results in a stronger resisting force to delamination, and a stagnant-lid may persist.

Systems of fractures in rifted lithosphere on Venus are an ideal environment for PBD to occur, because there is a pre-existing lithospheric weakness. We propose a new age-dependent framework for regional-scale lithospheric recycling at rift zones on Venus which includes both plume-induced and buoyancy-driven PBD. A young or recently thinned lithosphere may not be sufficiently negatively buoyant to undergo spontaneous PBD, but may be destabilized by a plume with a large buoyancy force. Yet as the plate ages and thickens, little or no plume interaction is needed to destabilize the rift margin. This indicates a certain inevitability of recycling rift-adjacent lithosphere via delamination processes, provided a weakness in the lithosphere persists. Although the rift margin may heal as the lithosphere ages and thickens, increasing plume buoyancy force is shown to drive destabilization in narrower, more stable margins. Plume-induced fracturing of off-axis lithosphere may be another mechanism of introducing weakness in thicker lithosphere (Schubert & Sandwell, 1995), which can provide a starting point for future delamination events. Our models provide a rough estimate of the amount of time a lithospheric weakness could exist before being destabilized by a direct encounter by a rising mantle plume. Due to potentially large variability in crust and lithosphere thickness, rift structure, and expected plume buoyancy force, different forms of PBD may operate independently at different times and in different locations on Venus. Currently, the Dali-Diana Chasmata system may be an ideal environment for delamination to occur due to its thick adjacent lithosphere. Rollback lithospheric recycling and internal rifting at Artemis Corona south of Diana Chasma may be evidence of a modern PBD event on Venus.

Data Availability Statement

The model data from this study are available in an online repository (Adams, 2023). StagYY (Tackley, 2008) is the property of P.J.T., and is available upon request for collaborative studies. Requests can be made to P.J.T (paul.tackley@erdw.ethz.ch). StagLab is available for access online (Crameri, 2021).

References

Adams, A. C. (2023). Plume-induced destabilization of rift zones on Venus. *Zenodo*. https://doi.org/10.5281/zenodo.7734818

Adams, A. C., Stegman, D. R., Smrekar, S. E., & Tackley, P. J. (2022). Regional-scale lithospheric recycling on Venus via peel-back delamination. *Journal of Geophysical Research: Planets*, *127*(10), 1–23. https://doi.org/10.1029/2022JE007460

Anderson, F. S., & Smrekar, S. E. (2006). Global mapping of crustal and lithospheric thickness on Venus. *Journal of Geophysical Research*, *111*(E8), 1–20. https://doi.org/10.1029/2004JE002395

Arkani-Hamed, J. (1993). On the tectonics of Venus. *Physics of the Earth and Planetary Interiors*, *76*(1–2), 75–96. https://doi.org/10.1016/0031-9201(93)90056-F

Armann, M., & Tackley, P. J. (2012). Simulating the thermochemical magmatic and tectonic evolution of Venus's mantle and lithosphere: Two-dimensional models. *Journal of Geophysical Research*, *117*(E12), 1–24. https://doi.org/10.1029/2012JE004231

Ashwal, L. D., Burke, K., & Sharpton, V. L. (1988). Lithospheric delamination on Earth and Venus. *Abstracts of the Lunar and Planetary Science Conference*, *19*, 17–18.

Azuma, S., Katayama, I., & Nakakuki, T. (2014). Rheological decoupling at the Moho and implication to Venusian tectonics. *Scientific Reports*, *4*, 1–5. https://doi.org/10.1038/srep04403

Basilevsky, A. T., & Head, J. W. (1998). The geologic history of Venus: A stratigraphic view. *Journal of Geophysical Research*, *103*(E4), 8531–8544. https://doi.org/10.1029/98je00487

Bird, P. (1979). Continental delamination and the Colorado plateau. *Journal of Geophysical Research*, *84*(B13), 7561–7571. https://doi.org/10.1029/JB084iB13p07561

Bjonnes, E. E., Hansen, V. L., James, B., & Swenson, J. B. (2012). Equilibrium resurfacing of Venus: Results from new Monte Carlo modeling and implications for Venus surface histories. *Icarus*, *217*(2), 451–461. https://doi.org/10.1016/j.icarus.2011.03.033

Buck, W. R. (1992). Global decoupling of crust and mantle: Implications for topography, geoid and mantle viscosity on Venus. *Geophysical Research Letters*, *9*(21), 2111–2114. https://doi.org/10.1029/92GL02462

Bullock, M. A., Grinspoon, D. H., & Head, J. W. (1993). Venus resurfacing rates: Constraints provided by 3-D Monte Carlo simulations. *Geophysical Research Letters*, *20*(19), 2147–2150. https://doi.org/10.1029/93GL02505

Chen, J., Jiang, H., Tang, M., Hao, J., Tian, M., & Chu, X. (2022). Venus' light slab hinders its development of planetary-scale subduction. *Nature Communications*, *13*, 1–9. https://doi.org/10.1038/s41467-022-35304-3

Chowdhury, P., Chakraborty, S., Gerya, T. V., Cawood, P. A., & Capitanio, F. A. (2020). Peel-back controlled lithospheric convergence explains the secular transitions in Archean metamorphism and magmatism. *Earth and Planetary Science Letters*, *538*, 1–13. https://doi.org/10.1016/j.epsl.2020.116224

Crameri, F. (2018). Geodynamic diagnostics, scientific visualisation and staglab 3.0. *Geoscientific Model Development*, *11*(6), 2541–2562. https://doi.org/10.5194/gmd-11-2541-2018

Crameri, F. (2021). Staglab. *Zenodo*. https://doi.org/10.5281/zenodo.5005427

Crameri, F., Lithgow-Bertelloni, C. R., & Tackley, P. J. (2017). The dynamical control of subduction parameters on surface topography. *Geochemistry, Geophysics, Geosystems*, *18*(4), 1661–1687. https://doi.org/10.1002/2017GC006821

Darold, A., & Humphreys, E. (2013). Upper mantle seismic structure beneath the pacific northwest: A plume-triggered delamination origin for the Columbia river flood basalt eruptions. *Earth and Planetary Science Letters*, *365*, 232–242. https://doi.org/10.1016/j.epsl.2013.01.024

Davaille, A., Smrekar, S. E., & Tomlinson, S. (2017). Experimental and observational evidence for plume-induced subduction on Venus. *Nature Geoscience*, *10*(5), 349–355. https://doi.org/10.1038/ngeo2928

Dombard, A. J., Johnson, C. L., Richards, M. A., & Solomon, S. C. (2007). A magmatic loading model for coronae on Venus. *Journal of Geophysical Research*, *112*(E4), 1–13. https://doi.org/10.1029/2006JE002731

Dupeyrat, L., & Sotin, C. (1995). The effect of the transformation of basalt to eclogite on the internal dynamics of Venus. *Planetary and Space Science*, *43*(7), 909–921. https://doi.org/10.1016/0032-0633(94)00227-i

Faccenda, M., Minelli, G., & Gerya, T. V. (2009). Coupled and decoupled regimes of continental collision: Numerical modeling. *Earth and Planetary Science Letters*, *278*(3–4), 337–349. https://doi.org/10.1016/j.epsl.2008.12.021

Feuvre, M. L., & Wieczorek, M. A. (2011). Nonuniform cratering of the Moon and a revised crater chronology of the inner solar system. *Icarus*, *214*, 1–20. https://doi.org/10.1016/j.icarus.2011.03.010

Gerya, T. V. (2014). Plume-induced crustal convection: 3D thermomechanical model and implications for the origin of novae and coronae on Venus. *Earth and Planetary Science Letters*, *391*, 183–192. https://doi.org/10.1016/j.epsl.2014.02.005

Ghail, R. (2015). Rheological and petrological implications for a stagnant lid regime on Venus. *Planetary and Space Science*, *113–114*, 2–9. https://doi.org/10.1016/j.pss.2015.02.005

Ghail, R. C. (2002). Structure and evolution of southeast Thetis Regio. *Journal of Geophysical Research*, *107*(E8), 1–7. https://doi.org/10.1029/2001je001514

Glaze, L. S., Stofan, E. R., Smrekar, S. E., & Baloga, S. M. (2002). Insights into corona formation through statistical analyses. *Journal of Geophysical Research*, *107*(E12), 1–12. https://doi.org/10.1029/2002je001904

Göğüş, O. H., Pysklywec, R. N., Şengör, A. M., & Gün, E. (2017). Drip tectonics and the enigmatic uplift of the central Anatolian plateau. *Nature Communications*, *8*, 1–9. https://doi.org/10.1038/s41467-017-01611-3

Göğüş, O. H., & Ueda, K. (2018). Peeling back the lithosphere: Controlling parameters, surface expressions and the future directions in delamination modeling. *Journal of Geodynamics*, *117*, 21–40. https://doi.org/10.1016/j.jog.2018.03.003

Gülcher, A. J., Gerya, T. V., Montési, L. G., & Munch, J. (2020). Corona structures driven by plume–lithosphere interactions and evidence for ongoing plume activity on Venus. *Nature Geoscience*, *13*(8), 547–554. https://doi.org/10.1038/s41561-020-0606-1

Hansen, V. L. (2002). Artemis: Surface expression of a deep mantle plume on Venus. *GSA Bulletin*, *7*, 839–848. https://doi.org/10.1130/0016-7606(2002)114⟨0839:ASEOAD⟩2.0.CO;2

Hoogenboom, T., & Houseman, G. A. (2006). Rayleigh-Taylor instability as a mechanism for corona formation on Venus. *Icarus*, *180*(2), 292–307. https://doi.org/10.1016/j.icarus.2005.11.001

Houseman, G. A., & Molnar, P. (1997). Gravitational (Rayleigh-Taylor) instability of a layer with non-linear viscosity and convective thinning of continental lithosphere. *Geophysical Journal International*, *128*(1), 125–150. https://doi.org/10.1111/j.1365-246X.1997.tb04075.x

Ito, K., & Kennedy, G. C. (1971). An experimental study of the basalt-garnet granulite-eclogite transition. *Geophysical Monograph Series*, *14*, 303–314. https://doi.org/10.1029/GM014p0303

Ivanov, M. A., & Head, J. W. (2011). Global geological map of Venus. *Planetary and Space Science*, *59*(13), 1559–1600. https://doi.org/10.1016/j.pss.2011.07.008

James, P. B., Zuber, M. T., & Phillips, R. J. (2013). Crustal thickness and support of topography on Venus. *Journal of Geophysical Research: Planets*, *118*(4), 859–875. https://doi.org/10.1029/2012JE004237

Janes, D. M., Squyres, S. W., Bindschadler, D. L., Baer, G., Schubert, G., Sharpton, V. L., & Stofan, E. R. (1992). Geophysical models for the formation and evolution of coronae on Venus. *Journal of Geophysical Research*, *97*(E10), 16055–16067. https://doi.org/10.1029/92je01689

Jiménez-Díaz, A., Ruiz, J., Kirby, J. F., Romeo, I., Tejero, R., & Capote, R. (2015). Lithospheric structure of Venus from gravity and topography. *Icarus*, *260*, 215–231. https://doi.org/10.1016/j.icarus.2015.07.020

Kargel, J. S., Komatsu, G., Baker, V. R., & Strom, R. G. (1993). The volcanology of Venera and VEGA landing sites and the geochemistry of Venus. *Icarus*, *103*(2), 253–275. https://doi.org/10.1006/icar.1993.1069

Katayama, I. (2021). Strength models of the terrestrial planets and implications for their lithospheric structure and evolution. *Progress in Earth and Planetary Science*, *8*, 1–17. https://doi.org/10.1186/s40645-020-00388-2

Koch, D. M., & Manga, M. (1996). Neutrally buoyant diapirs: A model for Venus coronae. *Geophysical Research Letters*, *23*(3), 225–228. https://doi.org/10.1029/95GL03776

Krystopowicz, N. J., & Currie, C. A. (2013). Crustal eclogitization and lithosphere delamination in orogens. *Earth and Planetary Science Letters*, *361*, 195–207. https://doi.org/10.1016/j.epsl.2012.09.056

Lourenço, D. L., Rozel, A. B., Ballmer, M. D., & Tackley, P. J. (2020). Plutonic-squishy lid: A new global tectonic regime generated by intrusive magmatism on Earth-like planets. *Geochemistry, Geophysics, Geosystems*, *21*(4), 1–24. https://doi.org/10.1029/2019GC008756

Mackwell, S. J., Zimmerman, M. E., & Kohlstedt, D. L. (1998). High-temperature deformation of dry diabase with application to tectonics on Venus. *Journal of Geophysical Research*, *103*(B1), 975–984. https://doi.org/10.1029/97JB02671

Magni, V., Faccenna, C., Hunen, J. V., & Funiciello, F. (2013). Delamination vs. break-off: The fate of continental collision. *Geophysical Research Letters*, *40*(2), 285–289. https://doi.org/10.1002/grl.50090

Martin, P., Stofan, E. R., Glaze, L. S., & Smrekar, S. (2007). Coronae of Parga Chasma, Venus. *Journal of Geophysical Research*, *112*(E4), 1–23. https://doi.org/10.1029/2006JE002758

McGovern, P. J., Rumpf, M. E., & Zimbelman, J. R. (2013). The influence of lithospheric flexure on magma ascent at large volcanoes on Venus. *Journal of Geophysical Research: Planets*, *118*(11), 2423–2437. https://doi.org/10.1002/2013JE004455

McKinnon, W. B., Zahnle, K. J., Ivanov, B. A., & Melosh, H. J. (1997). Cratering on Venus - Models and observations. *Venus II: Geology, Geophysics, Atmosphere, and Solar Wind Environment*, 969–1014.

Meissner, R., & Mooney, W. (1998). Weakness of the lower continental crust: A condition for delamination, uplift, and escape. *Tectonophysics*, *296*(1–2), 47–60. https://doi.org/10.1016/S0040-1951(98)00136-X

Ogawa, M., & Yanagisawa, T. (2014). Mantle evolution in Venus due to magmatism and phase transitions: From punctuated layered convection to whole-mantle convection. *Journal of Geophysical Research: Planets*, *119*(4), 867–883. https://doi.org/10.1002/2013JE004593

O'Rourke, J. G., & Smrekar, S. E. (2018). Signatures of lithospheric flexure and elevated heat flow in stereo topography at coronae on Venus. *Journal of Geophysical Research: Planets*, *123*(2), 369–389. https://doi.org/10.1002/2017JE005358

O'Rourke, J. G., Wolf, A. S., & Ehlmann, B. L. (2014). Venus: Interpreting the spatial distribution of volcanically modified craters. *Geophysical Research Letters*, *41*(23), 8252–8260. https://doi.org/10.1002/2014GL062121

Oxburgh, E. R., & Parmentier, E. M. (1977). Compositional and density stratification in oceanic lithosphere-causes and consequences. *Journal of the Geological Society*, *33*(4), 343–355. https://doi.org/10.1144/gsjgs.133.4.0343

Parmentier, E. M., & Hess, P. C. (1992). Chemical differentiation of a convecting planetary interior: Consequences for a one plate planet such as Venus. *Geophysical Research Letters*, *19*(20), 2015–2018. https://doi.org/10.1029/92GL01862

Phillips, R. J., Arvidson, R. E., Boyce, J. M., Campbell, D. B., Guest, J. E., Schaber, G. G., & Soderblom, L. A. (1991). Impact craters on Venus: Initial analysis from Magellan. *Science*, *252*(5003), 288–297. https://doi.org/10.1126/science.252.5003.288

Phillips, R. J., Raubertas, R. F., Arvidson, R. E., Sarkar, I. C., Herrick, R. R., Izenberg, N., & Grimm, R. E. (1992). Impact craters and Venus resurfacing history. *Journal of Geophysical Research*, *97*(E10), 923–938. https://doi.org/10.1029/92JE01696

Piskorz, D., Elkins-Tanton, L. T., & Smrekar, S. E. (2014). Coronae formation on Venus via extension and lithospheric instability. *Journal of Geophysical Research: Planets*, *119*(12), 2568–2582. https://doi.org/10.1002/2014JE004636

Regorda, A., Thieulot, C., Zelst, I. V., Erdős, Z., & Buiter, S. (2023). Rifting Venus: Insights from numerical modeling. *Journal of Geophysical Research: Planets*, *128*, 1–36. https://doi.org/10.1029/2022JE007588

Rolf, T., Steinberger, B., Sruthi, U., & Werner, S. C. (2018). Inferences on the mantle viscosity structure and the post-overturn evolutionary state of Venus. *Icarus*, *313*, 107–123. https://doi.org/10.1016/j.icarus.2018.05.014

Romeo, I., & Turcotte, D. L. (2009). The frequency-area distribution of volcanic units on Venus: Implications for planetary resurfacing. *Icarus*, *203*(1), 13–19. https://doi.org/10.1016/j.icarus.2009.03.036

Russell, M. B., & Johnson, C. L. (2021). Evidence for a locally thinned lithosphere associated with recent volcanism at aramaiti corona, Venus. *Journal of Geophysical Research: Planets*, *126*(8), 1–19. https://doi.org/10.1029/2020JE006783

Sandwell, D. T., Johnson, C. L., Bilotti, F., & Suppe, J. (1997). Driving forces for limited tectonics on Venus. *Icarus*, *129*(1), 232–244. https://doi.org/10.1006/icar.1997.5721

Sandwell, D. T., & Schubert, G. (1992a). Evidence for retrograde lithospheric subduction on Venus. *Science*, *257*(5071), 766–770. https://doi.org/10.1126/science.257.5071.766

Sandwell, D. T., & Schubert, G. (1992b). Flexural ridges, trenches, and outer rises around coronae on Venus. *Journal of Geophysical Research*, *97*(E10), 16069–16083. https://doi.org/10.1029/92je01274

Schaber, G. G., Strom, R. G., Moore, H. J., Soderblom, L. A., Kirk, R. L., Chadwick, D. J., et al. (1992). Geology and distribution of impact craters on Venus: What are they telling us? *Journal of Geophysical Research*, *97*(E8), 257–270. https://doi.org/10.1029/92JE01246

Schools, J., & Smrekar, S. E. (2023). High resolution numerical models of corona formation integrating magmatic processes, surface fracturing, and eclogitization. In *Proceedings of the 54th lunar and planetary science conference*.

Schubert, G., & Sandwell, D. (1995). A global survey of possible subduction sites on Venus. *Icarus*, *117*(1), 173–196. https://doi.org/10.1006/icar.1995.1150

Simons, M., Solomon, S. C., & Hager, B. H. (1997). Localization of gravity and topography: Constraints on the tectonics and mantle dynamics of Venus. *Geophysical Journal International*, *131*(1), 24–44. https://doi.org/10.1111/j.1365-246X.1997.tb00593.x

Smrekar, S. E., Hoogenboom, T., Stofan, E. R., & Martin, P. (2010). Gravity analysis of Parga and Hecate chasmata: Implications for rift and corona formation. *Journal of Geophysical Research*, *115*(E7), 1–19. https://doi.org/10.1029/2009JE003435

Smrekar, S. E., Ostberg, C., & O'Rourke, J. G. (2022). Earth-like lithospheric thickness and heat flow on Venus consistent with active rifting. *Nature Geoscience*, *16*(1), 13–18. https://doi.org/10.1038/s41561-022-01068-0

Smrekar, S. E., & Stofan, E. R. (1997). Corona formation and heat loss on Venus by coupled upwelling and delamination. *Science*, *277*(5330), 1289–1294. https://doi.org/10.1126/science.277.5330.1289

Solomatov, V. S., & Moresi, L. N. (1996). Stagnant lid convection on Venus. *Journal of Geophysical Research*, *101*(E2), 4737–4753. https://doi.org/10.1029/95JE03361

Solomon, S. C., Smrekar, S. E., Bindschadler, I. L. D., Grimm, R. E., Kaula, W. M., McGill, G. E., et al. (1992). Venus tectonics: An overview of Magellan observations. *Journal of Geophysical Research*, *97*(E8), 13199–13255. https://doi.org/10.1029/92JE01418

Spencer, J. E. (2001). Possible giant metamorphic core complex at the center of Artemis corona, Venus. *GSA Bulletin*, *10*(3), 333–345. https://doi.org/10.1130/0016-7606(2001)113⟨0333:PGMCCA⟩2.0.CO;2

Squyres, S. W., Janes, D. M., Baer, O., Bindschadler, D. L., Schubert, G., Sharpton, V. L., & Stofan, E. R. (1992). The morphology and evolution of coronae on Venus. *Journal of Geophysical Research*, *97*(E8), 611–624. https://doi.org/10.1029/92JE01213

Stofan, E. R., Bindschadler, D. L., Head, J. W., & Parmentier, E. M. (1991). Corona structures on Venus: Models of origin. *Journal of Geophysical Research*, *96*(E4), 20933–20946. https://doi.org/10.1029/91je02218

Stofan, E. R., Sharpton, V. L., Schubert, G., Baer, G., Bindschadler, D. L., Janes, D. M., & Squyres, S. W. (1992). Global distribution and characteristics of coronae and related features on Venus: Implications for origin and relation to mantle processes. *Journal of Geophysical Research*, *97*(E8), 13347–13378. https://doi.org/10.1029/92je01314

Strom, R. G., Schaber, G. G., & Dawson, D. D. (1994). The global resurfacing of Venus. *Journal of Geophysical Research*, *99*(E5), 899–909. https://doi.org/10.1029/94JE00388

Surkov, Y. A., Barsukov, V. L., Moskalyeva, L. P., Kharyukova, V. P., & Kemurdzhian, A. L. (1984). New data on the composition, structure, and properties of Venus rock obtained by Venera 13 and Venera 14. *Journal of Geophysical Research*, *89*(S02), 393–402. https://doi.org/10.1029/jb089is02p0b393

Surkov, Y. A., Moskalyova, L. P., Kharyukova, V. P., Dudin, A. D., Smirnov, G. G., & Zaitseva, S. Y. (1986). Venus rock composition at the Vega 2 landing site. *Journal of Geophysical Research*, *91*(B13), E215–E218. https://doi.org/10.1029/jb091ib13p0e215

Tackley, P. J. (2008). Modelling compressible mantle convection with large viscosity contrasts in a three-dimensional spherical shell using the yin-yang grid. *Physics of the Earth and Planetary Interiors*, *171*(1–4), 7–18. https://doi.org/10.1016/j.pepi.2008.08.005

Tackley, P. J., & Stevenson, D. J. (1991). The production of small Venusian coronae by Rayleigh-Taylor instabilities in the uppermost mantle. *EOS Transactions*, *72*, 287.

Thiriet, M., Breuer, D., Michaut, C., & Plesa, A. C. (2019). Scaling laws of convection for cooling planets in a stagnant lid regime. *Physics of the Earth and Planetary Interiors*, *286*, 138–153. https://doi.org/10.1016/j.pepi.2018.11.003

Tian, J., Tackley, P. J., & Lourenço, D. L. (2023). The tectonics and volcanism of Venus: New modes facilitated by realistic crustal rheology and intrusive magmatism. *Icarus*, *399*, 1–19. https://doi.org/10.1016/j.icarus.2023.115539

Turcotte, D. L. (1993). An episodic hypothesis for Venusian tectonics. *Journal of Geophysical Research*, *98*(E9), 61–78. https://doi.org/10.1029/93JE01775

Ueda, K., Gerya, T. V., & Burg, J. P. (2012). Delamination in collisional orogens: Thermomechanical modeling. *Journal of Geophysical Research*, *117*(B8), 1–25. https://doi.org/10.1029/2012JB009144

Uppalapati, S., Rolf, T., Crameri, F., & Werner, S. C. (2020). Dynamics of lithospheric overturns and implications for Venus's surface. *Journal of Geophysical Research: Planets*, *125*(11), 1–29. https://doi.org/10.1029/2019JE006258

Wallner, H., & Schmeling, H. (2010). Rift induced delamination of mantle lithosphere and crustal uplift: A new mechanism for explaining Rwenzori Mountains' extreme elevation? *International Journal of Earth Sciences*, *99*(7), 1511–1524. https://doi.org/10.1007/s00531-010-0521-6

Zuber, M. T. (1987). Constraints on the lithospheric structure of Venus from mechanical models and tectonic surface features. *Journal of Geophysical Research*, *92*(B4), E541–E551. https://doi.org/10.1029/JB092iB04p0E541